LASER
& PHOTONICS
REVIEWS

Laser Photonics Rev. **11,** No. 1, 1600263 (2017) / **DOI** 10.1002/lpor.201600263

Abstract Here we report on the hybrid nanostructures where a single ZnS nanobelt was half-covered with an aluminum (Al) film, which is an ideal platform for studying the second-harmonic generation (SHG) enhancement effects of the Al coating. It was fabricated by the lift-off process and allowed for the accurate comparison of the SHG intensity between the Al-covered and the same bare ZnS nanobelt under consistent test conditions. The results indicate that the Al coating in the hybrid nanostructures not only confines the pumping laser in the ZnS effectively, but also concentrates the emitted SHG signal greatly, increasing the signal collection efficiency. By the combination of these two effects, ~60 times enhancement of the SHG intensity is achieved at the optimized geometry size (width and thickness) of the ZnS nanobelts. The Al-based hybrid nanostructures open up new possibilities for low-cost, highly efficient and directional coherent nanolight sources at short wavelengths.

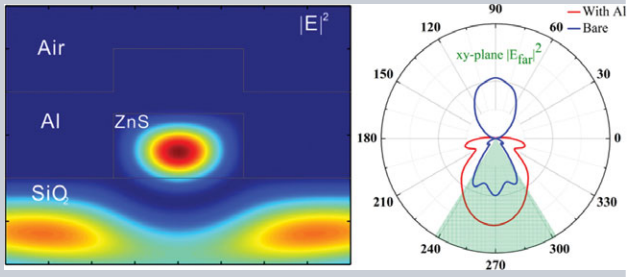

ORIGINAL
PAPER

Concentrated second-harmonic generation from a single Al-covered ZnS nanobelt

Hongbo Hu[1], Kai Wang[1,*], Hua Long[1], Xiaobo Han[1], Jiawei Chen[1], Bing Wang[1,*], and Peixiang Lu[1,2,*]

1. Introduction

A tunable nanoscale coherent light source is one of the key components for integrated nanophotonic systems. It has been realized in the ternary alloy CdS_xSe_{1-x} nanowire that covers from green to near-infrared region [1]. Tuning the spectral region to the shorter wavelength is important for high-precision detection [2, 3], high-resolution bio-imaging [4–6], and novel nanophotonic devices [7]. Second-harmonic generation (SHG) is a second-order nonlinear optical phenomenon that directly generates photons with half the incident wavelength, which has many merits such as wavelength tunability, nonthreshold, coherence, and ultrafast response [8, 9]. It provides a convenient method to obtain ultraviolet coherent light sources. Semiconductor nanowires or nanobelts are easy to grow and integrate, which have become one of the most promising building blocks for nanophotonic devices [10, 11]. Because of the excellent electrical and nonlinear optical properties of semiconductors, the SHG in semiconductor nanowires such as ZnO [12, 13], ZnTe [14], CdS [15], and GaAs [16] have drawn a lot of attention. Among them, zinc sulfide (ZnS) has a wide bandgap (3.7 eV) with a large exciton binding energy (40 meV) [17]. It is transparent in the near-ultraviolet, visible and near-infrared regions with large refractive indices ($n = 2.3$–2.5), which has been proved as an excellent material for short wavelength SHG [18].

Due to the diminutive scales of nanostructures, the SH signals radiated from the nanostructures are usually very weak [19]. Enhancing the nonlinear processes in nanostructures is a crucial step toward the practical applications of nanophotonic devices [20]. Many studies aimed at enhancing SHG in nanostructures have been proposed to overcome this severe limitation [15,21–30]. Typically, the noble metal–semiconductor (such as Au–CdS [15, 29], Au–ZnO [24], Au–GaAs [25], and Ag–ZnO [28]) hybrid nanostructures were fabricated to enhance SHG. Although Au and Ag are ideal surface plasmonic metals for the visible and near-infrared regions, they suffer high losses for the SH signals at short wavelengths [31–33]. Another important limitation is that the SH signals radiated from nanostructures are highly diverging due to the inherent diffraction effect [34, 35]. This goes against the effective utilization of the signal in integrated nanophotonic devices [36]. Compared with Au and Ag, Al has a broader plasmon resonant band that extends to ultraviolet region because its d-band lies above the Fermi energy [37, 38], which means that the Al can effectively confine the pumping laser, and generate a strong local-field enhancement. In addition, for the high reflectance in the ultraviolet region [39], a certain Al nanostructure can remarkably concentrate the emitted SH signals. Moreover, the stability of Al is comparable with the noble metals for the protection of compact oxide layer formed on its surface [40]. Therefore, replacing noble metal with Al in the metal–semiconductor hybrid nanostructures is of great meaning for enhancing SHG. It is worth noting that, for an accurate evaluation of the SHG enhancement factor of such hybrid nanostructures, the same single nanowire or nanobelt with and without a metal coating is highly required to be measured simultaneously under the same test conditions.

In this paper, we fabricated Al–ZnS hybrid nanostructures by the lift-off process, which allows us to cover one

[1] Wuhan National Laboratory for Optoelectronics and School of Physics, Huazhong University of Science and Technology, Wuhan 430074, China
[2] Laboratory of Optical Information Technology, Wuhan Institute of Technology, Wuhan 430205, China
*Corresponding authors: e-mail: kale_wong@hust.edu.cn; wangbing@hust.edu.cn; lupeixiang@hust.edu.cn

© 2016 by WILEY-VCH Verlag GmbH & Co. KGaA, Weinheim

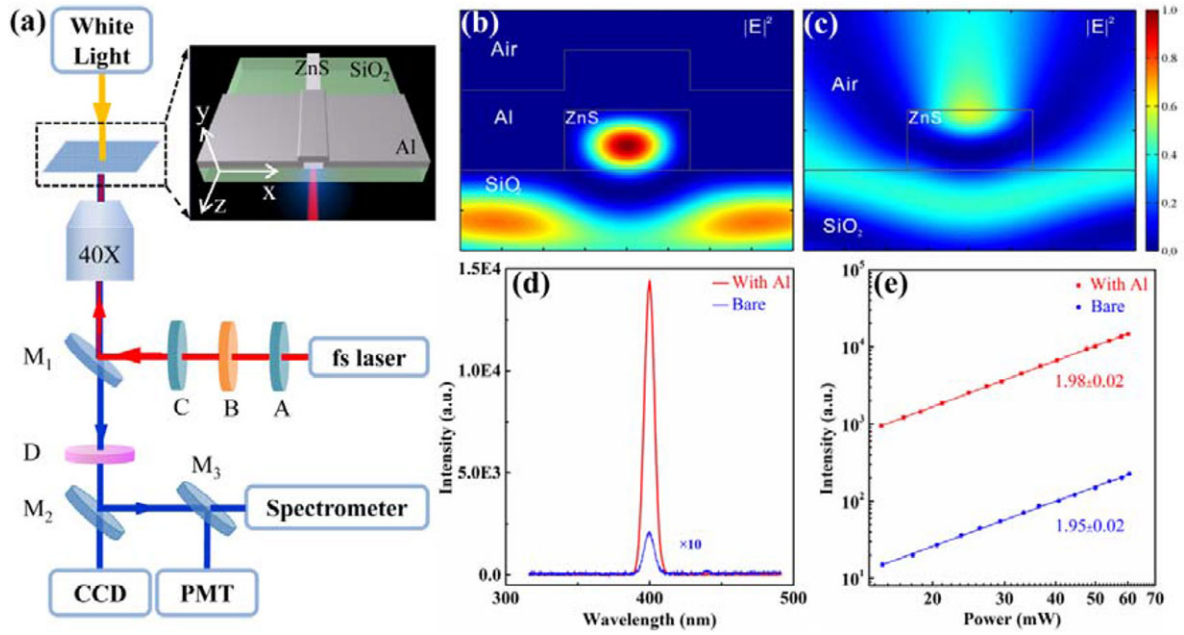

Figure 1 (a) The schematic sketch of the setup used for SHG measurements with a backscattering geometry. A femtosecond laser (50 fs, 76 MHz) centered at 800 nm was used as the excitation source. **A** and **B** are half-wave plate and polarizing beam splitter, respectively, which were used to adjust the intensity of the pumping laser. The polarization direction of the laser was controlled by another half-wave plate, **C**. $\mathbf{M_1}$ is an ultrafast mirror that has the reflection region ranges from 700 to 930 nm, and is transparent to most visible light. The sample was placed on a two-dimensional motorized stage. **D** is a 720 nm short-pass filter. The backscattering signal was collected by the same objective and subsequently imported to the CCD, PMT, or spectrometer. $\mathbf{M_2}$ and $\mathbf{M_3}$ are UV enhanced aluminum mirrors that mounted on the flip mount adapter. The ZnS nanobelt lying on the quartz substrate is half-covered by an Al film. The femtosecond laser was focused onto the ZnS nanobelt through the quartz substrate with the polarized direction parallel (TM) or vertical (TE) to the growth axis of the ZnS nanobelts. (b, c) Calculated intensity distribution ($\boldsymbol{I}_\omega = |\boldsymbol{E}_\omega|^2$) patterns of the pumping laser in the cross section of the samples (with and without Al) under TM pumping. (d) Spectra of the signals radiated from the Al-covered (red line) and the same bare (blue line, multiplied by 10) ZnS nanobelt. The peaks centered at 400 nm are exactly the double frequency of the fundamental laser. (e) Emitted signal intensity as a function of the pumping power on a log–log scale. The red dots represent the results for the Al-covered ZnS nanobelt and the blue dots represent those for the same bare nanobelt. The solid lines show a linear fit with a slope about 2, indicating the square dependence between the signal intensity and the pumping power.

part of a ZnS nanobelt with Al film. It provides an ideal platform for comparing the SHG intensity between the Al-covered and the same bare ZnS nanobelt simultaneously, which guarantees the same test conditions for an accurate evaluation of the SHG enhancement effects. The Al-covered ZnS nanobelts can be regarded as an Al nanocavity that is filled with ZnS, which can effectively confine and enhance the pumping laser within the ZnS. In addition, a great concentration of the SH signals induced by the nanocavity enhances the collection efficiency. An SHG enhancement exceeding a factor of 60 was achieved from the Al-covered ZnS. The experiment and simulation analyses manifest that the SHG enhancement effects are influenced not only by the polarization of the pumping laser, but also by the geometry sizes (width and thickness) of ZnS nanobelts.

2. Experiment methods

The single-crystalline ZnS nanobelts used in the experiments were synthesized by the chemical vapor deposition (CVD) method [18]. The widths of the ZnS nanobelts are about 200 to 800 nm, and the thicknesses are about 60 to 130 nm. A lift-off process was used to fabricate the Al-covered ZnS nanobelts. The detailed steps are: first, a quartz substrate on which the ZnS nanobelts disperse goes through standard photolithography treatments, namely photoresist coating, exposure, and developing. Then, an Al film with a thickness of about 200 nm is deposited onto the quartz substrate by electron beam evaporation. Due to the good adhesion between the Al layer and quartz [38], no additional adhesion layer was required. Finally, after removing the remaining photoresist with acetone, the Al film covered on the photoresist will be removed automatically and the designed microstructure is left on the substrate.

The optical measurements were carried out at room temperature by an inverted microscope (IX73, Olympus) configured with a two-dimension motorized stage (BIOS-L101T-S, SIGMAKOKI). As shown in Fig. 1a, a mode-locked Ti-sapphire femtosecond laser centered at 800 nm (Tsunami, Spectra-Physics, 50 fs and 76 MHz) was focused onto the ZnS nanobelt through the quartz substrate by a 40× objective (Olympus, NA 0.55). The polarized direction of

© 2016 by WILEY-VCH Verlag GmbH & Co. KGaA, Weinheim

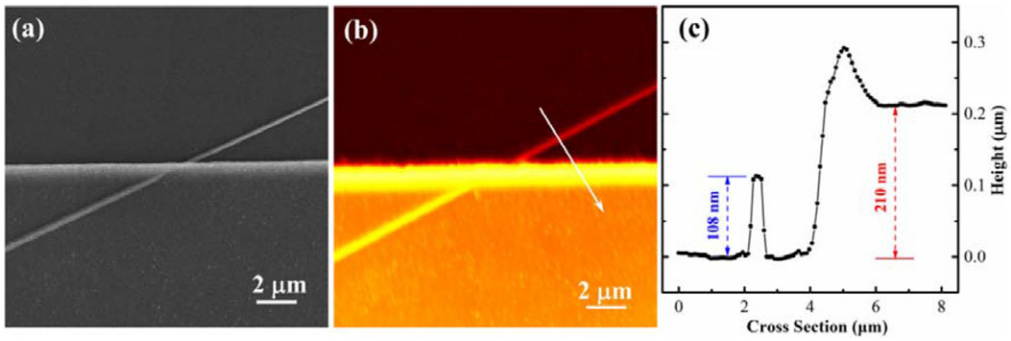

Figure 2 (a) SEM image of the hybrid nanostructure, where a straight ZnS nanobelt with a smooth surface lies on the quartz substrate. A part of the ZnS nanobelt is covered by an Al film and the remaining part remains bare. The width of the nanobelt is measured to be 250 nm. (b) Corresponding AFM image of the same area in (a). (c) Cross-sectional profile extracted from the white line in (b). The thicknesses of the ZnS nanobelt and the Al film are determined to be 108 nm and 210 nm, respectively.

the laser was parallel (TM) or vertical (TE) to the growth axis of the ZnS nanobelt. The backscattering SH signal was collected by the same objective. The spectrum and the intensity of SHG were measured by a spectrometer (Princeton Instruments Acton 2500i with CCD camera Pixis 400) and a Photomultiplier (PMT, Hamamatsu H7827) after removing the pumping laser with a short-pass filter (Semrock, SP 720 nm).

The morphology of ZnS nanobelts and the hybrid nanostructures were characterized by the field-emission scanning electron microscope (FESEM, Nova NanoSEM 450) and the atom force microscope (AFM, Veeco NanoScope MultiMode). X-ray diffraction (XRD, X'Pert PRO, PANalytical B.V., Netherlands) and high-resolution transmission electron microscopy (HRTEM, Tecnai G220) were used to measure the crystal structure of the ZnS nanobelts (shown in Fig. S1 in the Supporting Information). As for the physical model, a commercial finite element software (Comsol Multiphysics) was used for the simulation analyses.

3. Results and discussion

In order to study the enhancement effect of the Al–ZnS hybrid nanostructure, the SHG intensity at two different positions that are bare and Al-covered on the same ZnS nanobelt were compared. Figure 1d shows the spectra of the signals radiated from a single ZnS nanobelt with (red curve) and without Al coating (blue curve). The peak intensity from the Al-covered ZnS is about 60 times higher than that from the same bare one, implying that the emitted signal is strongly enhanced by the Al coating. The sharp peak centered at 400 nm is exactly the double frequency of the pumping laser. Figure 1e presents the signal intensities as a function of the pumping power for both Al-covered ZnS nanobelt (red dots) and the same bare nanobelt (blue dots). The slopes from the log–log plots indicate the quadratic relationship between the signal intensity and the pumping power, which confirms that the emitted signal is ascribed to the SHG process. It should be noted that there was no measurable SH signal from the Al film or the quartz substrate when the pumping laser was only focused on them, indicating that the active material radiating SHG is the ZnS nanobelt. To understand the enhancement mechanism, a two-dimensional model was built to calculate the average intensity of fundamental laser inside the ZnS nanobelt (shown in Fig. S5 in the supporting information). The typical calculated intensity distribution patterns in the ZnS nanobelt with and without Al are shown in Fig. 1b and 1c, respectively. It can be seen that the Al coating serves as a nanocavity that is filled with ZnS, and the pumping laser is effectively confined in the cavity. Therefore, the average intensity in the Al-covered ZnS is enhanced in comparison with the bare nanobelt.

The morphology of the hybrid nanostructures was characterized by SEM, and it is found that all the ZnS nanostructures used in our experiment were nanobelts with rectangle cross sections (shown in the supporting information Fig. S1). Figure 2a shows a typical SEM image of the Al–ZnS hybrid nanostructure. A straight ZnS nanobelt with a smooth surface lies on the substrate, and a part of the nanobelt is covered by the Al film and the remaining part remains bare. The width of the nanobelt is 250 nm measured from the SEM image. As shown in Fig. 2b, the corresponding AFM image was also obtained to measure the thicknesses of the ZnS nanobelt and the Al film. The cross-sectional profile (Fig. 2c) extracted from the white line in Fig. 2b shows that the thicknesses of the nanobelt and the Al film are 108 nm and 210 nm, respectively. As is shown by the AFM image, the edge of the Al film is a little upturned, which may be caused by the final step of the lift-off process when removing the redundant Al. Since this situation only occurs at the edge of an Al film to a small degree, it would not affect the comparison of the SHG enhancement in our experiment.

For a more accurate estimation of the SHG enhancement factor, the corresponding SHG scanning images on the same area in Fig. 2a were obtained. During the measurement, the sample was placed on the motorized stage that moves automatically with a scanning step of 300 nm, and the femtosecond laser was focused to a spot with a

© 2016 by WILEY-VCH Verlag GmbH & Co. KGaA, Weinheim

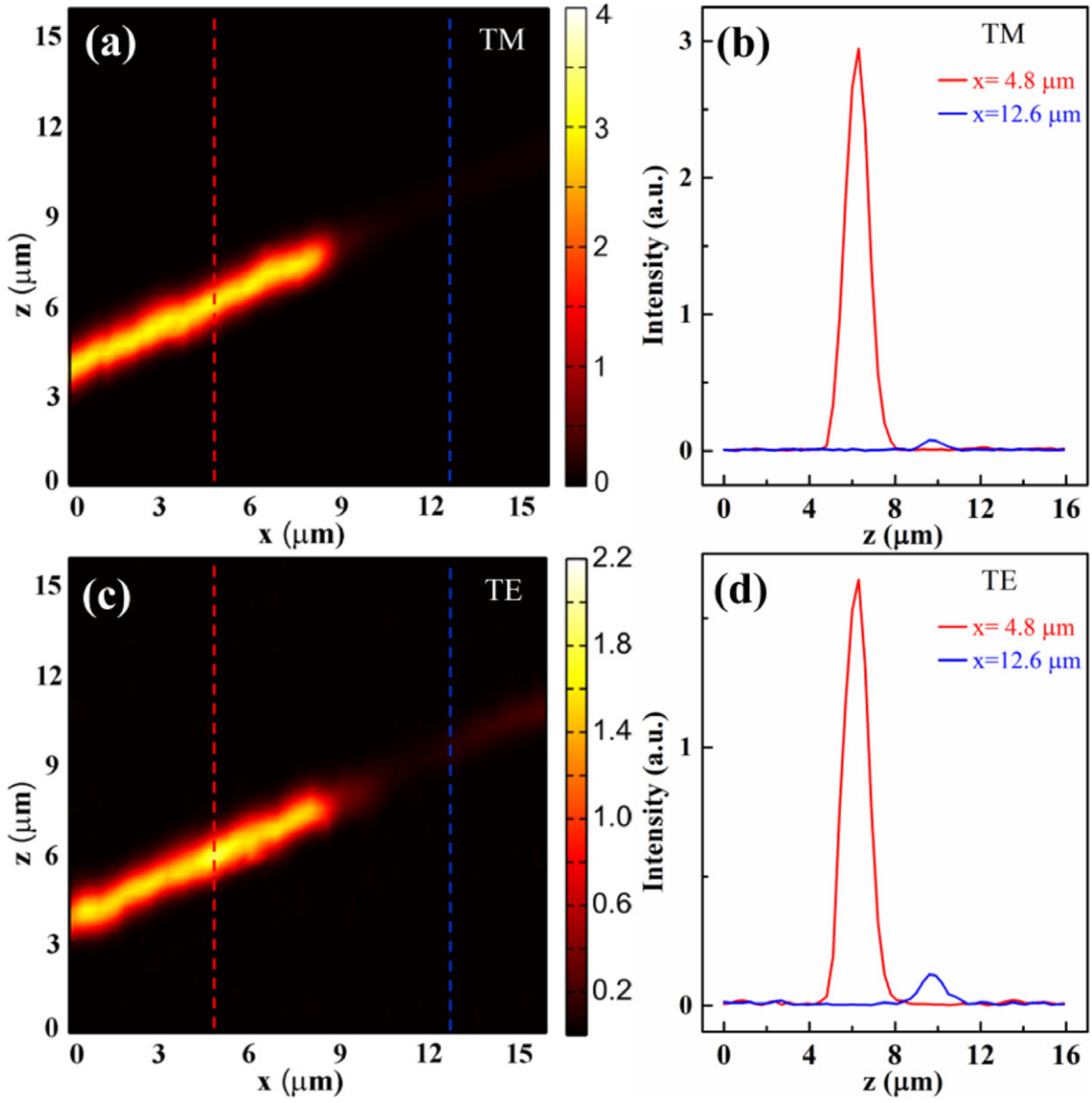

Figure 3 (a, c) The corresponding SHG scanning images of the same area shown in Fig. 2a under TM and TE pumping, respectively, which were obtained by moving the sample with a motorized stage. The SHG intensities from the Al-covered part are much stronger than the bare part. (b, d) Line profiles extracted from the red and blue dashed lines in the SHG scanning images in (a) and (c), respectively. The peak of the red solid line shows the SHG intensity of the Al-covered ZnS nanobelt, and the peak of the blue solid line shows that of the bare part. The SHG enhancement factors are 34- and 12-fold under TM and TE pumping, respectively.

diameter of about 3 μm. Figures 3a and 3c show the SHG scanning images under TM and TE polarization pumping, respectively. It shows that the ZnS nanobelt with an Al coating possesses a much stronger SHG intensity than the bare part. Both parts have a stable and uniform SHG intensity distribution along the nanobelt, and no SHG was observed in the Al film background or underlying substrate. As the line profiles shown in Figs. 3b and 3d that are extracted from the corresponding SHG scanning images, the SHG enhancement factors are 34 and 12 times under TM and TE polarization pumping, respectively. In our experiment, tens of Al-covered ZnS nanobelts with different cross sections were studied. It is found that the SHG enhancement factors are influenced by the polarization of the pumping laser and the geometry size (width and thickness) of ZnS nanobelts.

The ZnS used in the experiment is wurtzite crystal structure that belongs to the 6*mm* space group [18], it is a noncentrosymmetric crystal that allows for bulk SHG. Because the intensity of the SH signal has a quadratic relationship to the pumping power, the intensity of the pumping laser inside the ZnS nanobelt is crucial to estimate the SHG enhancement. By the finite-element method, the average intensities

© 2016 by WILEY-VCH Verlag GmbH & Co. KGaA, Weinheim

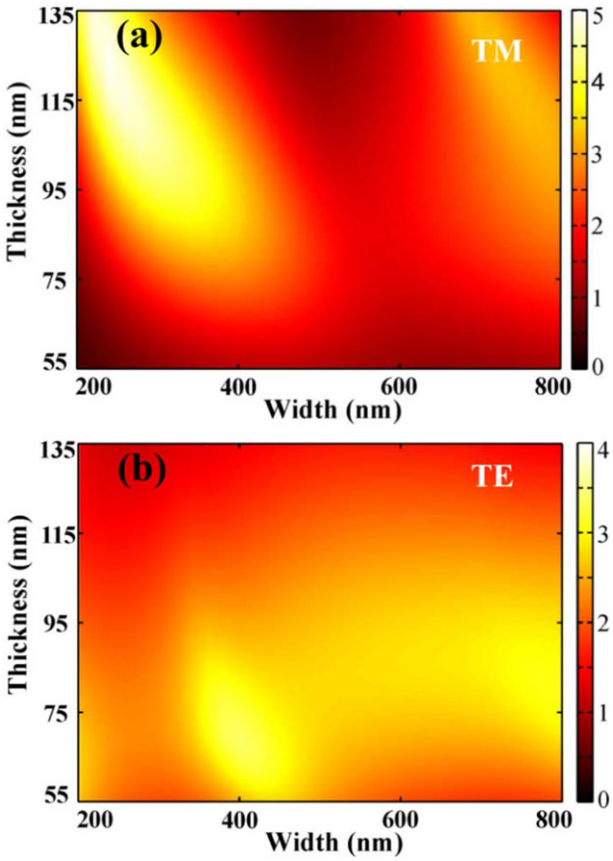

Figure 4 Calculated local-field enhancement factors for the pumping laser inside the ZnS under TM (a) and TE (b) pumping, which vary with the changes of nanobelts geometry sizes. The data are obtained by dividing the average intensity of the pumping laser inside the Al-covered nanobelt with that of the same bare one.

of the pumping laser confined in the ZnS were calculated for nanobelts with different geometry sizes. According to the sizes of the ZnS nanobelts used in our experiment, the size parameters for calculations are ranged from 200 nm to 800 nm in width, and from 55 nm to 135 nm in thickness. Dividing the average intensity of the pumping laser in the Al-covered ZnS nanobelt by that in the same bare nanobelt, the local-field enhancement factors are obtained for nanobelts with different widths and thicknesses under TM and TE pumping, which are shown in Figs. 4a and 4b, respectively. In general, the local-field intensity inside an Al-covered ZnS nanobelt is significantly enhanced for both TM and TE polarizations. The Al coating in the hybrid nanostructures serves as a nanocavity that effectively confines the pumping laser, leading to the strong local-field enhancement. As can be seen in Fig. 4a, for certain sizes of nanobelts, the pumping laser resonates in the nanocavity, and therefore generates a higher local-field intensity with the largest enhancement factor of about 5.

There is another important factor that the SHG collection efficiency should be considered for evaluating the SHG enhancement. Since the SH signals are collected by an objective with a collection cone angle of about 67 degrees (40×, 0.55 NA), a certain amount of the SH signals will radiates without collecting especially for the highly divergent emissions. As discussed, the Al coating in the hybrid nanostructure has a high reflectance for the SH signals, and forms a nanocavity that is filled with ZnS. Therefore, it would efficiently concentrate the SH signals emitted from the ZnS nanobelt, and consequently increase the signal collection efficiency of the objective. The SHG radiated from nanocrystals can be regarded as electrical dipoles that oscillate at doubled frequency [41, 42], and the main dipole components collected by the objective are polarized in the ***xz***-plane of the laboratory coordinate. A three-dimensional model was built based on the electric dipole approximation method to evaluate the signal collection efficiency (shown in the supporting information Fig. S6). A point electric dipole at doubled frequency (400 nm) with TE or TM polarization was placed in the center of a ZnS nanobelt, and the related far-field radiation patterns were calculated. Figures 5a and 5b present the typical far-field radiation patterns of the Al-covered and the bare ZnS nanobelt with TM and TE polarization, respectively. As can be seen, the SH signals radiated from the Al-covered nanobelt are greatly concentrated, which can be collected efficiently by the objective. The collection efficiency is determined by the ratio between the far-field intensity ($|E_{\mathrm{far}}|^2$) radiation within the collection cone and the total far-field intensity. By comparing the collection efficiency for the structure with and without Al coating, the enhancements of the SHG collection efficiency are obtained.

Owing to the combination of the two effects, namely the local-field enhancement for the pumping laser and the collection efficiency enhancement for the SH signals, a significant SHG enhancement is achieved in the Al-covered ZnS nanobelt in comparison with the bare nanobelt. According to the simulation analyses above, the total enhancement factor $\boldsymbol{F}_{\mathrm{t}}$ is defined as:

$$F_{\mathrm{t}} = F_{\omega}^{2} \cdot F_{2\omega}, \tag{1}$$

where $\boldsymbol{F}_{\omega}$ is the local-field enhancement factor for the pumping laser, and $\boldsymbol{F}_{2\omega}$ represents the collection efficiency enhancement factor for the SHG. As shown in Fig. 4, the $\boldsymbol{F}_{\omega}$ varies with the geometry sizes of ZnS nanobelts, which leads to the variation of the total enhancement factor. Specifically, in the resonance condition for pumping laser, $\boldsymbol{F}_{\omega}$ is maximized as 5-fold, take the $\boldsymbol{F}_{2\omega}$ of about 3-fold at this resonance geometry size into consideration, the total SHG enhancement factor is estimated to be about 75-fold. Table 1 presents the enhancement results of several Al-covered ZnS nanobelts with different cross-sectional sizes. The widths and thicknesses of the ZnS nanobelts were determined by the corresponding SEM and AFM images, and the theoretical SHG enhancement factors are calculated by Eq. (1). As shown in Table 1, the calculated results are consistent with the experimental observations. The good agreements further confirm the contributions of these two effects to the SHG enhancement in the hybrid nanostructure.

© 2016 by WILEY-VCH Verlag GmbH & Co. KGaA, Weinheim

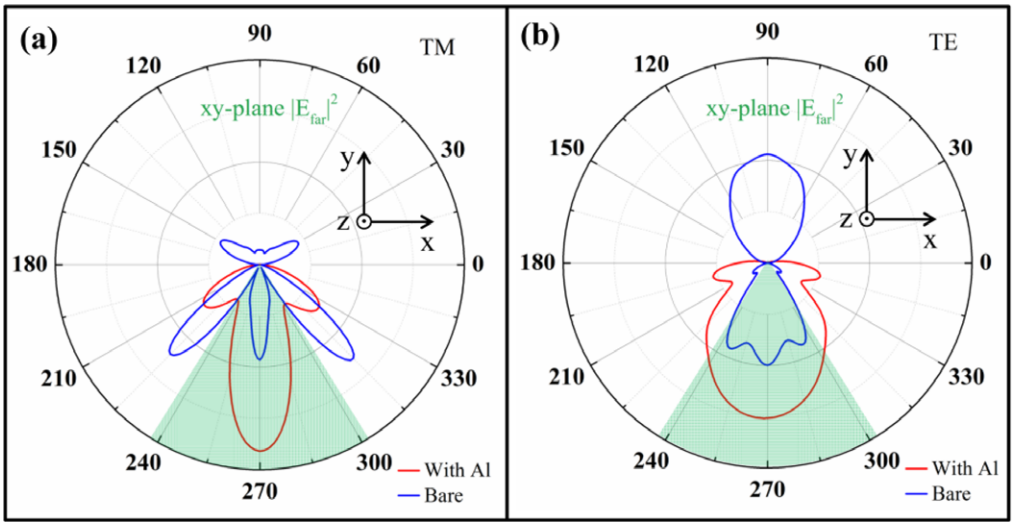

Figure 5 The polar plots of the far-field intensity $|E_{far}|^2$ distribution of the SH signal in the *xy*-plane. The width and thickness of the simulated nanobelt are 260 nm and 120 nm, respectively. (a) Calculated far-field scattering patterns of the SH signals with the TM (along the *z*-axis) polarization. The green area shows the collection cone of the objective. (b) Calculated far-field scattering patterns of the SH signals with the TE (along the *x*-axis) polarization.

Table 1 The SHG enhancement factors measured in the experiment for the different sizes of ZnS nanobelts. The calculated enhancement values are also listed in the table, which are in good agreement with the experimental results.

Number	Width [nm]	Thickness [nm]	SHG Enhancement			
			TM		TE	
			Exp	$\boldsymbol{F}_{\omega}{}^2 \cdot \boldsymbol{F}_{2\omega} = \boldsymbol{F}_{t}$	Exp	$\boldsymbol{F}_{\omega}{}^2 \cdot \boldsymbol{F}_{2\omega} = \boldsymbol{F}_{t}$
1	214	98	18.9	$2.52^2 \times 2.56 = 16.2$	3.1	$1.91^2 \times 1.07 = 3.9$
2	250	108	34.0	$4.38^2 \times 1.89 = 36.2$	12.0	$1.67^2 \times 1.28 = 3.6$
3	260	120	66.2	$4.80^2 \times 3.36 = 77.4$	6.8	$1.43^2 \times 1.22 = 2.5$
4	370	100	26.1	$3.75^2 \times 1.56 = 22.0$	12.0	$2.32^2 \times 1.59 = 8.6$
5	390	88	19.3	$3.45^2 \times 1.43 = 17.0$	12.7	$2.78^2 \times 1.68 = 13.0$
6	406	83	16.4	$3.21^2 \times 1.54 = 15.9$	17.3	$2.93^2 \times 1.86 = 16.0$
7	416	93	18.4	$3.13^2 \times 2.07 = 20.3$	11.4	$2.55^2 \times 1.64 = 10.7$
8	418	97	17.6	$3.01^2 \times 2.38 = 21.5$	11.5	$2.42^2 \times 1.66 = 9.7$
9	580	90	6.7	$1.74^2 \times 1.81 = 5.5$	10.1	$2.79^2 \times 1.16 = 9.0$
10	650	86	10.2	$1.98^2 \times 2.19 = 8.6$	8.7	$2.85^2 \times 1.16 = 9.4$

Except for the SHG enhancement effect, the Al-covered ZnS hybrid nanostructure provides a promising platform for many other applications. For example, the interval between the Al stripes fabricated in our experiment is 30 μm, which is close to the length of the ZnS nanobelts. It is easy for us to make Al electrodes on both ends of the nanobelt. In consideration of the excellent electrical and optical properties of ZnS, the hybrid nanostructure can work as functional optoelectronic devices such as ultraviolet photodetectors, electro-optic modulators, and THz emitters based on the optical rectification effect. As is well known, it is difficult to couple photons into surface plasmon polaritons (SPPs) for the difficulty to realize phase-matching condition [36, 43]. The frequency-doubled signals generated in the Al–ZnS hybrid nanostructure may have the potential to serve as the effective SPPs pumping sources at short wavelengths.

4. Conclusions

In summary, we present a novel hybrid nanostructure where a single ZnS nanobelt was half-covered with an Al film by

© 2016 by WILEY-VCH Verlag GmbH & Co. KGaA, Weinheim

the lift-off process. It provides an ideal platform for comparing the SHG intensity between the Al-covered and the same bare ZnS nanobelt simultaneously, which guarantees the same test conditions for an accurate evaluation. The SHG enhancement exceeding a factor of 60 was achieved at the optimized geometry size of the ZnS nanobelts. It was found that the Al coating in the hybrid nanostructures acts as a nanocavity that effectively confines the pumping laser and generates a strong local-field enhancement. In addition, the nanocavity increases the signal-collection efficiency by greatly concentrating the emitted SHG. The simulation results further support the experimental data. The Al-based hybrid nanostructure is a promising candidate for a highly efficient and directional coherent nanolight source that has many potential applications in ultraviolet photodetectors, electro-optic modulators in the short-wavelength region.

Supporting Information

Additional supporting information may be found in the online version of this article at the publisher's website.

Acknowledgements. This work was supported by the 973 Programs under grants 2014CB921301 and the National Natural Science Foundation of China (11204097), the Doctoral fund of the Ministry of Education of China under Grant No. 20130142110078, the Fundamental Research Funds for the Central Universities, HUST: 2016YXMS015. Special thanks to the Analytical and Testing Center of HUST and the Center of Micro-Fabrication and Characterization (CMFC) of WNLO for use of their facilities.

Received: 3 October 2016, **Revised:** 11 November 2016, **Accepted:** 22 November 2016

Published online: 16 December 2016

Key words: aluminum, zinc sulfide nanobelts, second-harmonic generation, enhancement, nanolight source.

References

[1] A. Pan, W. Zhou, E. S. P. Leong, R. Liu, A. H. Chin, B. Zou, and C. Ning, Nano Lett. **9**, 784–788 (2009).
[2] Y. Nakayama, P. J. Pauzauskie, A. Radenovic, R. M. Onorato, R. J. Saykally, J. Liphardt, and P. Yang, Nature **447**, 1098–1102 (2007).
[3] R. Kolkowski, J. Szeszko, B. Dwir, E. Kapon, and J. Zyss, Opt. Express **22**, 30592–30606 (2014).
[4] N. Olivier, M. A. Luengo-Oroz, L. Duloquin, E. Faure, T. Savy, I. Veilleux, X. Solinas, D. Debarre, P. Bourgine, A. Santos, N. Peyrieras, and E. Beaurepaire, Science **329**, 967–971 (2010).
[5] P. J. Campagnola, and C.Y. Dong, Laser Photon. Rev. **5**, 13–26 (2011).
[6] F. Cai, J. Yu, J. Qian, Y. Wang, Z. Chen, J. Huang, Z. Ye, and S. He, Laser Photon. Rev. **8**, 865–874 (2014).
[7] C. J. Barrelet, H. S. Ee, S. H. Kwon, and H. G. Park, Nano Lett. **11**, 3022–3025 (2011).
[8] R. W. Boyd, Nonlinear Optics, 3rd edition, (Academic Press, Burlington, MA, USA, 2008).
[9] X. Yin, Z. Ye, D. A. Chenet, Y. Ye, K. O'Brien, J. C. Hone, and X. Zhang, Science **344**, 488–490 (2014).
[10] R. Yan, D. Gargas, and P. Yang, Nature Photon. **3**, 569–576 (2009).
[11] M. L. Ren, R. Agarwal, W. Liu, and R. Agarwal, Nano Lett. **15**, 7341–7346 (2015).
[12] S. K. Das, M. Bock, C. O'Neill, R. Grunwald, K. M. Lee, H. W. Lee, S. Lee, and F. Rotermund, Appl. Phys. Lett. **93**, 181112 (2008).
[13] X. Han, K. Wang, H. Long, H. Hu, J. Chen, B. Wang, and P. Lu, ACS Photon. **3**, 1308–1314 (2016).
[14] W. Liu, K. Wang, Z. Liu, G. Shen, and P. Lu, Nano Lett. **13**, 4224–4229 (2013).
[15] M. L. Ren, W. Liu, C. O. Aspetti, L. Sun, and R. Agarwal, Nature Commun. **5**, 5432 (2014).
[16] R. Grange, G. Bronstrup, M. Kiometzis, A. Sergeyev, J. Richter, C. Leiterer, W. Fritzsche, C. Gutsche, A. Lysov, W. Prost, F. J. Tegude, T. Pertsch, A. Tunnermann, and S. Christiansen, Nano Lett. **12**, 5412–5417 (2012).
[17] J. A. Zapien, Y. Jiang, X. M. Meng, W. Chen, F. C. K. Au, Y. Lifshitz, and S. T. Lee, Appl. Phys. Lett. **84**, 1189–1191 (2004).
[18] H. Hu, K. Wang, H. Long, W. Liu, B. Wang, and P. Lu, Nano Lett. **15**, 3351–3357 (2015).
[19] M. Cazzanelli, F. Bianco, E. Borga, G. Pucker, M. Ghulinyan, E. Degoli, E. Luppi, V. Veniard, S. Ossicini, D. Modotto, S. Wabnitz, R. Pierobon, and L. Pavesi, Nature Mater. **11**, 148–154 (2012).
[20] Y. Pu, R. Grange, C. L. Hsieh, and D. Psaltis, Phys. Rev. Lett. **104**, 207402 (2010).
[21] R. Kolkowski, J. Szeszko, B. Dwir, E. Kapon, and J. Zyss, Laser Photon. Rev. **10**, 287–298 (2016).
[22] K. Thyagarajan, S. Rivier, A. Lovera, and O. J. F. Martin, Opt. Express **20**, 12860–12865 (2012).
[23] D. Lehr, J. Reinhold, I. Thiele, H. Hartung, K. Dietrich, C. Menzel, T. Pertsch, E.-B. Kley, and A. Tuennermann, Nano Lett. **15**, 1025–1030 (2015).
[24] G. Grinblat, M. Rahmani, E. Cortes, M. Caldarola, D. Comedi, S. A. Maier, and A. V. Bragas, Nano Lett. **14**, 6660–6665 (2014).
[25] A. Casadei, E. F. Pecora, J. Trevino, C. Forestiere, D. Rueffer, E. Russo-Averchi, F. Matteini, G. Tutuncuoglu, M. Heiss, A. Fontcuberta i Morral, and L. Dal Negro, Nano Lett. **14**, 2271–2278 (2014).
[26] A. Sergeyev, R. Geiss, A. S. Solntsev, A. A. Sukhorukov, F. Schrempel, T. Pertsch, and R. Grange, ACS Photon. **2**, 687–691 (2015).
[27] S. Kruk, M. Weismann, A. Y. Bykov, E. A. Mamonov, I. A. Kolmychek, T. Murzina, N. C. Panoiu, D. N. Neshev, and Y. S. Kivshar, ACS Photon. **2**, 1007–1012 (2015).
[28] J. K. Hyun, T. Kang, H. Baek, H. Oh, D.-S. Kim, and G.-C. Yi, ACS Photon. **2**, 1314–1319 (2015).
[29] X. Liu, Q. Zhang, W. K. Chong, J. N. Yip, X. Wen, Z. Li, F. Wei, G. Yu, Q. Xiong, and T. C. Sum, ACS Nano **9**, 5018–5026 (2015).
[30] R. Kolkowski, L. Petti, M. Rippa, C. Lafargue, and J. Zyss, ACS Photon. **2**, 899–906 (2015).
[31] S. Lal, S. Link, and N. J. Halas, Nature Photon. **1**, 641–648 (2007).

© 2016 by WILEY-VCH Verlag GmbH & Co. KGaA, Weinheim

[32] G. V. Naik, V. M. Shalaev, and A. Boltasseva, Adv. Mater. **25**, 3264–3294 (2013).
[33] J. M. McMahon, G. C. Schatz, and S. K. Gray, Phys. Chem. Chem. Phys. **15**, 5415–5423 (2013).
[34] N. Yang, W. E. Angerer, and A. G. Yodh, Phys. Rev. Lett. **87**, 103902 (2001).
[35] C. I. Valencia, E. R. Mendez, and B. S. Mendoza, J. Opt. Soc. Am. B **21**, 36–44 (2004).
[36] D. K. Gramotnev and S. I. Bozhevolnyi, Nature Photon. **4**, 83–91 (2010).
[37] M. W. Knight, N. S. King, L. Liu, H. O. Everitt, P. Nordlander, and N. J. Halas, ACS Nano **8**, 834–840 (2014).
[38] M. W. Knight, L. Liu, Y. Wang, L. Brown, S. Mukherjee, N. S. King, H. O. Everitt, P. Nordlander, and N. J. Halas, Nano Lett. **12**, 6000–6004 (2012).
[39] Y. Ekinci, H. H. Solak, and J. F. Loffler, J. Appl. Phys. **104**, 083107 (2008).
[40] C. Langhammer, M. Schwind, B. Kasemo, and I. Zoric, Nano Lett. **8**, 1461–1471 (2008).
[41] W. E. Angerer, N. Yang, A. G. Yodh, M. A. Khan, and C. J. Sun, Phys. Rev. B **59**, 2932–2946 (1999).
[42] C. L. Hsieh, Y. Pu, R. Grange, and D. Psaltis, Opt. Express **18**, 11917–11932 (2010).
[43] S. Ke, B. Wang, C. Qin, H. Long, K. Wang, and P. Lu, J. Lightwave Technol. **34**, 5258–5262 (2016).

© 2016 by WILEY-VCH Verlag GmbH & Co. KGaA, Weinheim